JGR Biogeosciences

RESEARCH ARTICLE
10.1029/2019JG005558

Special Section:
Carbon cycling in tidal wetlands and estuaries of the contiguous United States

Carbon Dioxide and Methane Emissions From A Temperate Salt Marsh Tidal Creek

Branimir Trifunovic[1], Alma Vázquez-Lule[1], Margaret Capooci[1], Angelia L. Seyfferth[1], Carlos Moffat[2], and Rodrigo Vargas[1]

[1]Department of Plant and Soil Sciences, College of Agriculture and Natural Resources, University of Delaware, Newark, DE, USA, [2]School of Marine Science and Policy, College of Earth, Ocean, and Environment, University of Delaware, Newark, DE, USA

Abstract Coastal salt marshes store large amounts of carbon but the magnitude and patterns of greenhouse gas (GHG; i.e., carbon dioxide (CO_2) and methane (CH_4)) fluxes are unclear. Information about GHG fluxes from these ecosystems comes from studies of sediments or at the ecosystem-scale (eddy covariance) but fluxes from tidal creeks are unknown. We measured GHG concentrations in water, water quality, meteorological parameters, sediment CO_2 efflux, ecosystem-scale GHG fluxes, and plant phenology; all at half-hour intervals over 1 year. Manual creek GHG flux measurements were used to calculate gas transfer velocity (k) and parameterize a model of water-to-atmosphere GHG fluxes. The creek was a source of GHGs to the atmosphere where tidal patterns controlled diel variability. Dissolved oxygen and wind speed were negatively correlated with creek CH_4 efflux. Despite lacking a seasonal pattern, creek CO_2 efflux was correlated with drivers such as turbidity across phenological phases. Overall, nighttime creek CO_2 efflux (3.6 ± 0.63 μmol/m^2/s) was at least 2 times higher than nighttime marsh sediment CO_2 efflux (1.5 ± 1.23 μmol/m^2/s). Creek CH_4 efflux (17.5 ± 6.9 nmol/m^2/s) was 4 times lower than ecosystem-scale CH_4 fluxes (68.1 ± 52.3 nmol/m^2/s) across the year. These results suggest that tidal creeks are potential hotspots for CO_2 emissions and could contribute to lateral transport of CH_4 to the coastal ocean due to supersaturation of CH_4 (>6,000 μmol/mol) in water. This study provides insights for modeling GHG efflux from tidal creeks and suggests that changes in tide stage overshadow water temperature in determining magnitudes of fluxes.

Key Points:
- A tidal creek was a hotspot for CO_2 efflux compared to the surrounding wetland
- Changes in tide stage, not water temperature variability, regulated diel creek CO_2 and CH_4 efflux
- The relative influence of nontidal drivers of creek CO_2 and CH_4 efflux varied by plant phenological phases

Supporting Information:
- Supporting Information S1

Correspondence to:
R. Vargas,
rvargas@udel.edu

Citation:
Trifunovic, B., Vázquez-Lule, A., Capooci, M., Seyfferth, A. L., Moffat, C., & Vargas, R. (2020). Carbon dioxide and methane emissions from a temperate salt marsh tidal creek. *Journal of Geophysical Research: Biogeosciences*, *125*, e2019JG005558. https://doi.org/10.1029/2019JG005558

Received 7 NOV 2019
Accepted 23 JUN 2020
Accepted article online 30 JUN 2020
Corrected 12 OCT 2020

This article was corrected on 12 OCT 2020. See the end of the full text for details.

Author Contributions:
Conceptualization: Branimir Trifunovic, Angelia L. Seyfferth, Rodrigo Vargas
Formal analysis: Branimir Trifunovic
Funding acquisition: Rodrigo Vargas
Investigation: Branimir Trifunovic, Alma Vázquez-Lule, Margaret Capooci
Methodology: Branimir Trifunovic, Carlos Moffat, Rodrigo Vargas
Project administration: Rodrigo Vargas
(continued)

1. Introduction

Coastal salt marshes are becoming increasingly of interest for carbon cycle science due to the large amounts of carbon sequestered in their sediments (Howard et al., 2017). These systems are disproportionately important to the global carbon cycle relative to their small global area (22,000–400,000 km^2); on average they store 10 times more carbon per unit area than terrestrial forests (McLeod et al., 2011) and possess high concentrations of CO_2 and CH_4 at depth (Seyfferth et al., 2020). However, this carbon reservoir is sensitive to changes in wetlands including increased erosion and decomposition due to sea level rise (Jones et al., 2018; Ruiz-Fernández et al., 2018), habitat disturbance from land cover change and seagrass accumulation, (Macreadie et al., 2013; Pendleton et al., 2012), and increased heterotrophic respiration due to rising temperatures (Bond-lamberty et al., 2018; Kirwan et al., 2014). The vulnerability of these large carbon stocks requires detailed research into the magnitudes, patterns, and drivers of carbon exchange across different landscape features in salt marshes.

Coastal salt marshes are hotspots for carbon storage because they are suboxic to anoxic, which decreases the rate of heterotrophic decomposition of soil organic carbon (SOC). In wet sediments, limited oxygen supply drives anaerobic metabolism by soil microbes, which lowers CO_2 emissions compared to upland terrestrial environments where aerobic metabolism dominates (Greenwood, 1961; Raich & Schlesinger, 1992). Moreover, sulfate-reducing bacteria compete with methanogens for substrate during acetoclastic and hydrogenotrophic methanogenesis, thereby lowering CH_4 production via this pathway (Tobias & Neubauer, 2009). That said, recent work suggests that in sulfate-rich marsh sediments, methanogenesis may proceed via methylotrophic methanogenesis where sulfate-reducing bacteria do not compete for substrate and this can result in high concentrations of gaseous CH_4 at depth (Seyfferth et al., 2020). The slow rate of carbon oxidation in marsh sediments results in large accumulations of SOC within these ecosystems

Resources: Angelia L. Seyfferth, Rodrigo Vargas
Supervision: Angelia L. Seyfferth, Rodrigo Vargas
Writing - original draft: Branimir Trifunovic
Writing – review & editing: Alma Vázquez-Lule, Margaret Capooci, Angelia L. Seyfferth, Carlos Moffat, Rodrigo Vargas

(Chmura et al., 2003). However, there is a delicate balance between anaerobic and aerobic conditions in these tidal systems due to the tidal ebb and flood, which lowers the water table elevation and increases the redox potential of the sediments near tidal channels (Baumann et al., 2015; Seyfferth et al., 2020). These dynamic conditions could promote emissions of CO_2 and CH_4 from the land surface and water-to-atmosphere via changes in oxygen concentrations and redox oscillations (Moseman-Valtierra, 2012). Therefore, understanding the patterns and drivers of salt marsh greenhouse gas (GHG; i.e., CO_2 and CH_4) efflux is important to understand how SOC in salt marshes will respond to weather variability and global environmental change.

The majority of salt marsh GHG efflux studies have focused on soils/sediment (Capooci et al., 2019; Chmura et al., 2011; Tong et al., 2010, 2013; Seyfferth et al., 2020) or used eddy covariance towers at ecosystem-scale (Forbrich et al., 2018; Forbrich & Giblin, 2015; Moffett et al., 2010), but the dynamics of GHG efflux from tidal creeks are currently unknown. Past studies on soil GHG fluxes revealed that tidal patterns play an important role in GHG dynamics in these ecosystems. These tidal patterns affect both CO_2 (Huertas et al., 2017) and CH_4 emissions (Tong et al., 2010) by increasing the aerobic zone in the sediment profile near tidal creeks with the ebbing tide and decreasing the aerobic zone with the flooding tide. Furthermore, GHG-enriched porewater and groundwater has been observed to be tidally transported in estuarine systems as well (Sadat-Noori et al., 2015; Santos et al., 2012), and tides also affect the conditions for GHG efflux by moving sediments, organic matter, and nutrients into and out of the marsh (Fagherazzi et al., 2013). Despite the knowledge of tides as an important GHG efflux control, to our knowledge there have been no studies of GHG efflux directly from marsh tidal channels or creeks. These landscape features have been shown to be important sources of dissolved inorganic carbon to estuaries (Neubauer & Anderson, 2003; Wang et al., 2016; Wang & Cai, 2004), and may be important contributors of CH_4 and CO_2 efflux in marsh ecosystems.

Previous studies on GHG efflux from terrestrial streams, mangrove tidal creeks, and coastal rivers found that flowing waters have high GHG efflux and suggest that GHG efflux from salt marsh creeks could be higher per unit area than the surrounding landscape (Call et al., 2015; Lauerwald et al., 2015; Linto et al., 2014; Raymond et al., 2013; Yang et al., 2017). Therefore, our overarching goal was to characterize the temporal dynamics and the magnitude of the CO_2 and CH_4 efflux from a temperate salt marsh tidal creek. A crucial part of this goal was characterizing marsh plant phenology, as phenology has been determined to have a strong influence on carbon dynamics across wetland ecosystems (Desai, 2010; Kang et al., 2016; Vázquez-Lule et al., 2019) and thus is a strong seasonal control on salt marsh GHG dynamics. In particular, we aimed to (a) measure the temporal patterns and magnitudes of CO_2 and CH_4 efflux from a salt marsh creek; (b) identify the biophysical drivers for CO_2 and CH_4 efflux throughout the year; and (c) determine how the magnitudes of CO_2 and CH_4 efflux compare to those from sediments and at the ecosystem-scale.

We explored four interrelated hypotheses: First, we hypothesized that creek GHG emissions would be higher in the peak of the growing season (i.e., maturity phenophase) due to increased plant and microbial heterotrophic respiration (Zhong et al., 2013) and methanogenesis (Yvon-Durocher et al., 2014) as a result of higher temperature and organic matter supply from plant development. Second, water-to-atmosphere GHG efflux would be highest during ebb and flood tides as the water is moving faster (and higher rates of turbulence are expected) compared to the low flows at high and low tides. This hypothesis is supported by the fact that faster water velocity usually has a higher gas transfer velocity (Raymond et al., 2012). Third, temporal patterns of CO_2 and CH_4 may be autocorrelated with each other due to the shared influence of phenology, temperature, and tides as mentioned in Hypotheses 1 and 2; however, dissolved oxygen and salinity will likely be stronger negative controls on CH_4 emissions due to their inhibiting effect on methanogenesis (Poffenbarger et al., 2011; Tobias & Neubauer, 2009). Fourth, the creek's CO_2 emissions (per unit area) could be higher than the surrounding soil emissions because of the high GHG efflux potential of flowing waters (Lauerwald et al., 2015; Linto et al., 2014). We addressed this research by taking advantage of automated measurements of CO_2 and CH_4 concentrations (alongside a wide array of ancillary information) which provided unprecedented information about temporal patterns of GHG emissions in tidal salt marshes.

2. Materials and Methods

2.1. Study Site

This study was carried out in the St. Jones Reserve, a component of the Delaware National Estuarine Research Reserve in Dover, Delaware, USA. The study site is part of the AmeriFlux (site ID: US-StJ) and Phenocam (site ID: stjones) networks. The GHG concentration and efflux sampling location was located at Aspen Landing within a microtidal (mean tide range of 1.5 m), mesohaline (typical salinity of 5–18 ppt) salt marsh (Delaware Department of Natural Resources and Environmental Control, 1999) tidal creek. The creek makes up 6.9% of the area of the study site (Figure S1 in the supporting information). *Spartina alterniflora* is the dominant plant species, making up 62.2% of the marsh's land cover with the invasive *Phragmites australis* representing 13.4% (Delaware Department of Natural Resources and Environmental Control, 1999). The reserve is located on the Atlantic Coastal Plain geologic unit (Delaware Department of Natural Resources and Environmental Control, 1999) and made up of 40% Transquaking and 40% Mispillon soils consisting of layers of mucky peat, muck, mucky silt loam, and silt loam (Soil Survey Staff NRCS, United States Department of Agriculture, 2019). The climate is temperate with four distinct seasons and an average maximum July temperature of 31.7°C and an average minimum January temperature of 4.4° C, and average precipitation is 117 cm/year with an average snowfall of 40 cm/year (Delaware Department of Natural Resources and Environmental Control, 1999).

2.2. Plant Phenophases

The plant phenophases were identified using the greenness index (GI), a vegetation index derived from a time lapse of red, green, and blue (i.e., RGB) photographs of vegetation cover that quantifies the number of green pixels relative to the overall brightness (Gillespie et al., 1987). Data were divided by phenophase as plant phenology: (a) determines primary productivity of terrestrial ecosystems (Flanagan, 2009; Richardson et al., 2010; Wu et al., 2013); (b) is closely related to carbon dynamics in wetland ecosystems (Desai, 2010; Kang et al., 2016; Vázquez-Lule et al., 2019); and (c) influences fluxes of dissolved organic carbon between salt marsh sediments and the water column (Dausse et al., 2012).

The study site follows the PhenoCam network's protocol for data collection, storage and processing (Seyednasrollah et al., 2019). A NetCam SC camera (StarDot Technologies, Buena Vista, CA, USA) took RGB photographs every half hour, and we identified a region of interest (ROI) adjacent to the creek as there was no plant growth within the creek. This ROI was chosen following standard guidelines of the PhenoCam network (Seyednasrollah et al., 2019). The ROI was represented mainly by *S. cynosuroides* with some *S. alterniflora*, a typical species composition near the creek banks of the Reserve. Phenocam data were analyzed from 3 March 2017 to 13 December 2017. Phenology data were reviewed, analyzed, and divided into phenophases using standard protocols defined by the Phenopix R package (Filippa et al., 2016). Data revision consisted of calculating the daily averages of the greenness index and filtering out images that were too dark. Four distinct phenophases were identified based on the greenness index: (a) *Dormant* for when the plants were inactive during winter; (b) *Greenup* for when the plants were initially growing following the *Dormant* phenophase; (c) *Maturity* for when the plants reached a peak in greenness; and (d) *Senescence* for when the plants started losing greenness as they moved into the *Dormant* phenophase.

2.3. Creek CO_2 and CH_4 Fluxes

The concentrations of CO_2 (pCO_2) and CH_4 (pCH_4) within the water of the creek were measured from 3 March 2017 to 13 December 2017. We used an eosGP CO_2 Concentration Probe (Eosense, Dartmouth, NS, Canada) with a calibration range of 0–20,000 μmol/mol, an equilibration time of <90 s, and an accuracy of ±200 μmol/mol, and a Mini-Pro CH_4 Probe (Pro Oceanus, Bridgewater, NS, Canada) with a calibration range of 0–10,000 μmol/mol, an equilibration time of 4 min, and an accuracy of ±200 μmol/mol. Data were collected every minute, corrected for changes in pressure and temperature, and averaged into 30-min intervals. Probes were cleaned with deionized water every 2 weeks to prevent sediment accumulation and biofilm buildup in the sensor membranes.

Manual measurements of CO_2 and CH_4 efflux from the creek were taken every 2 weeks from September 2017 to December 2017 along with four 24-hr sampling campaigns (two neap tides; 9/1/17, 11/9/17, two spring tides; 9/18/17, 11/3/17) to capture tidal diel patterns. Each campaign sampled over the course of two tidal cycles, with measurements at low, flood, high, and ebb tide, for a total of eight measurements.

Low tide was defined as the half hour before and after the local minima of the water level, while high tide used the local maxima. Each local minima and maxima were calculated using the Tides package in R (Cox & Schepers, 2017). Flood tide was assigned to all measurements taken after low tide but before high tide, and ebb tide was assigned to all measurements taken after high tide but before low tide. Low tide ranged from −0.26 to −0.16 m above sea level, flood and ebb tide ranged from −0.16 to 0.665 m above sea level, and high tide ranged from 0.665 to 1.16 m above sea level.

A closed-system floating flux chamber (20 cm in diameter) was coupled with an Ultraportable Greenhouse Gas Analyzer (Los Gatos Research, Santa Clara, CA, USA) with a range and error of 1–20,000 ± 0.3 ppm for CO_2 and 0.01–100 ± 0.002 ppm for CH_4 for flux measurements. GHG concentrations were automatically corrected for water vapor dilution (reporting dry CO_2 or dry CH_4 concentrations) within the Ultraportable Greenhouse Gas Analyzer. Each manual chamber measurement lasted 3 min to allow the gases to accumulate and the change in concentration within the chamber was recorded every 2 s by the Ultraportable Greenhouse Gas Analyzer. Creek GHG effluxes were calculated with a linear equation using the change in gas concentration over time, chamber volume and area, atmospheric pressure, water temperature, and the ideal gas law constant as described in previous studies (Pearson et al., 2016; Warner et al., 2017). Any linear regression with an r-squared of less than 0.9 was discarded as it was considered a low-quality measurement following a standard protocol (Capooci et al., 2019). Three consecutive manual measurements were taken and averaged to represent one measurement in time for subsequent analyses. A total of 38 averaged measurements were recorded and included to parameterize the final model.

2.4. Water-to-Atmosphere Flux Model

Automatic concentrations and manual flux measurements of each GHG were used with Equations 1 and 2 (Van Dam et al., 2019; Wanninkhof, 2014) to build a model of water-to-atmosphere GHG efflux from the tidal creek at a 30-min time step. First, the gas transfer velocity was calculated as

$$k = \frac{fGas(measured)}{\Delta pGas^{*}k_0} \quad (1)$$

where k is the gas transfer velocity (m/s), $\Delta pGas$ is the difference between the concentrations of the GHG of interest in the water and the atmosphere (μmol/mol), k_0 is the solubility coefficient of the GHG of interest (mol/L/atm) calculated based on temperature and gas pressure, and *fGas (measured)* is the measured flux (from manual measurements) of the GHG of interest (μmol/m^2/s). For each GHG, a k was calculated for each of the four tide stages using the mean of all measurements taken at each tide stage. Then *fGas (modeled),* representing the predicted GHG efflux (μmol/m^2/s), was calculated as

$$fGas(modeled) = k^{*}k_0^{*}\Delta pGas \quad (2)$$

where k is the gas transfer velocity for a specific tidal stage, and $\Delta pGas$ is the difference between the concentrations of the GHG of interest in the water and the concentration of the GHG in the atmosphere for a specific tidal stage (associated with the respective k). All parameters of the equation, save for the k constant, change based on input values (at a 30-min time step). Site-specific k values were used for the gas flux model calculation but standardized k_{600} values were calculated for easier comparison with other gas transfer studies using Equation 3 with n as 0.5 (Lorke et al., 2015) and a temperature and salinity-dependent Schmidt number (Sc; Wanninkhof, 2014):

$$k_{600} = k^{*}\left(\frac{600}{Sc}\right)^{-n} \quad (3)$$

Finally, all measurements underwent QA/QC (e.g., check for outliers, data inconsistencies) and we provide a 30-min time step and daily averages for further data analysis.

2.5. Ancillary Measurements

Ecosystem-scale CO_2 and CH_4 fluxes were measured by the Eddy Covariance (EC) technique. The EC tower is equipped with a WindMaster Pro anemometer, model 160724 (Gill Instruments, Lymington, Hamisphere, UK), a LI-7200RS enclosed path CO_2/H_2O Analyzer and a LI-7700 open path CH_4 analyzer, both sensors

from LI-COR (LI-COR Environmental, Lincoln, NE, USA). All data were collected at 10 Hz, processed in EddyPro 6.2.0 Software from LI-COR (LI-COR Environmental, Lincoln, NE, USA) and corrected for potential misalignments of the anemometer, turbulence fluctuations, and air density fluctuations following AmeriFlux protocols. For this study we used nighttime net ecosystem exchange (NEE) as a representation of ecosystem respiration (Barba et al., 2018; Mahecha et al., 2010) and compared it solely to nighttime soil and creek CO_2 efflux. All available data, both nighttime and daytime, were used for comparing ecosystem-scale CH_4 fluxes to creek CH4 fluxes.

Soil CO_2 fluxes (representing total soil respiration) were measured from bare sediments within a vegetated plot every 5 min with the eosFD Soil CO_2 Flux Sensor (Eosense, Dartmouth, NS, Canada) at two different locations—approximately 13 and 51 m from the creek bank. The chamber footprint measured 10.2 cm in diameter and measurements from both chambers were averaged together for all analyses. The eosFD uses forced diffusion to regulate gas flow through a diffusive membrane rather than a more traditional mechanical pump, as seen in other closed chamber setups (Risk et al., 2011). The water quality parameters (measured in 15 min intervals) of temperature, salinity, water level, turbidity, and dissolved oxygen were measured with a YSI 6600 sonde (YSI Inc., Yellow Springs, OH, USA) The weather parameters (measured in 15-min intervals) of barometric pressure, wind speed, total photosynthetically active radiation, and total precipitation, were measured with a CR1000 Meteorological Monitoring Station (Campbell Scientific, Logan, UT, USA). Both the water quality and weather parameters followed the Centralized Data Management Protocol from the National Estuarine Research Reserve System (NERRS) (Small et al., 2012). All measurements underwent QA/QC (e.g., check for outliers, data inconsistencies) and were averaged into a 30-min time step and daily averages for further data analysis.

2.6. Data Analysis

All data were processed and analyzed using R 3.4.3 (R Foundation for Statistical Computing, Vienna, Austria). Nonparametric Kruskal-Wallis tests followed by Dunn post hoc tests were used for all analyses involving manual GHG flux data. Parametric ANOVA tests followed by Tukey HSD post hoc tests were used for all other analyses.

A canonical correlation analysis (CCA) using the R *CCA* package (González & Déjean, 2012) was performed on daily averages to test the influence of various independent variables on the dependent variables of creek CO_2 and CH_4 efflux. This analysis is useful to identify and measure the associates of two sets of variables as multiple studies have recognized that there is a close association between CO_2 and CH_4 fluxes (Jamali et al., 2013; Knox et al., 2019; Vargas & Barba, 2019). Consequently, the CCA method was chosen so the correlation between CO_2 and CH_4 effluxes can be examined to determine how different independent variables may affect only one or both GHGs considering potential intercorrelations. One CCA was performed using all available data and one was carried out for each phenophase, making a total of five separate analyses. A p-value < 0.05 was used to determine if each CCA found a statistically significant relationship between the independent and dependent variables.

The independent variables consisted of temperature, salinity, water level, turbidity, dissolved oxygen, barometric pressure, wind speed, total photosynthetically active radiation, and total precipitation. The CCA reduced all the independent variables to one independent canonical variate, and all the dependent variables to one dependent canonical variate (Thomas, 1984). The relationship between all the independent and dependent variables was represented by a linear correlation coefficient calculated between the independent canonical variate and the dependent canonical variate. The contribution of each variable to that overall correlation was represented by the linear correlation coefficient calculated between that variable and its respective variate.

3. Results

Daily averages of ancillary measurements from March to December were typical of a Mid-Atlantic tidal salt marsh (Figure 1). The GI (unitless; 0.34 ± 0.02) peaked on DOY 219 (0.40; 08/07/17) with an initial *Dormant* phase of 116 days, a *Greenup* phenophase of 74 days, a short *Maturity* phenophase of 32 days, a *Senescence* phenophase of 78 days, and a second *Dormant* phenophase of 65 days (Figure 1a). Water temperature (Figure 1b; 17.6 ± 6.87°C) and GI roughly followed the same seasonal pattern, while dissolved oxygen

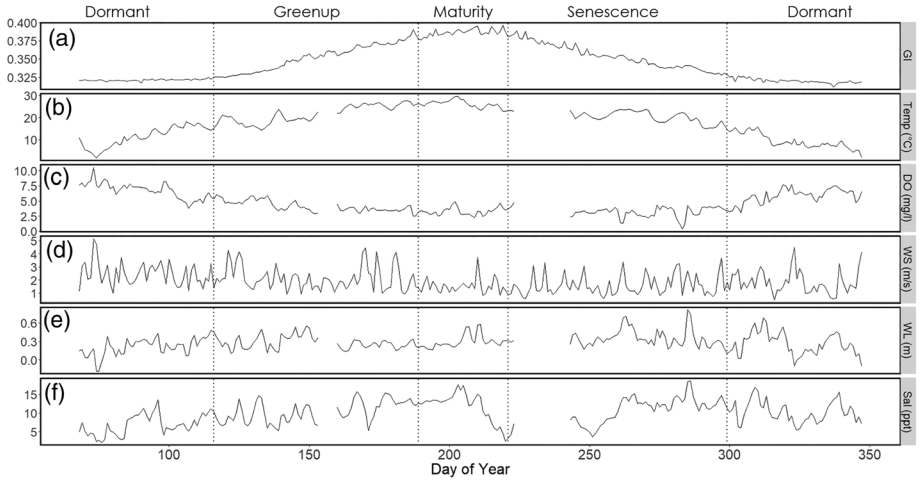

Figure 1. Time series of daily averages of greenness index (a), water temperature (b), dissolved oxygen (c), wind speed (d), water level above sea level (e), and salinity (f) during 2017. The time series are divided into *Dormant*, *Greenup*, *Maturity*, and *Senescence* phenophases marked by vertical dotted lines.

(Figure 1c; 4.62 ± 1.71 mg/l) showed an inverse pattern of being lowest in July (0.36 mg/L) when temperature (29.52°C) and GI (0.40) were highest. Other measured variables did not show a seasonal pattern, despite having differences among phenophases. Water level (Figure 1e); 0.28 m ± 0.12 above sea level), wind speed (Figure 1d; 1.9 ± 0.89 m/s), and salinity (Figure 1f; 10.0 ± 3.54 ppt) were dominated by shorter-period variability (days to weeks) pattern. Salinity did tend to increase slowly during the first half of the record, but no clear seasonal cycle was discernible. Data gaps in water quality data were due to annual servicing and cleaning of the YSI sensor (8.6% of the total data).

Modeled creek GHG effluxes were compared against the corresponding manual measurements. There were no statistically significant differences between means of modeled (CO_2; 3.88 ± 2.52 μmol/m^2/s, CH_4; 25.4 ± 21.6 nmol/m^2/s) and manual measurements (CO_2; 4.11 ± 4.51 μmol/m^2/s, CH_4; 28.71 ± 31.93 nmol/m^2/s) overall (i.e., all available measurements) and when analyzed for each tide stage (Kruskal-Wallis test; $p > 0.05$; Figure 2), but manual measurements had a larger range (CO_2; 0.26–20.1 μmol/m^2/s, CH_4; 1.3–123 nmol/m2/s) than modeled values (CO_2; 0.53–8.0 μmol/m^2/s, CH_4; 2.05–66.9 nmol/m^2/s). Due to the limited amount of manual measurements to independently test the model output, a bootstrap *t* test was also performed on modeled versus measured values and found no statistically significant differences between the means. The magnitude of both manual and modeled GHG fluxes decreased in the order low tide > ebb tide > flood tide > high tide (Kruskal-Wallis test; $p < 0.05$; Figure 2). Gas transfer velocities, standardized to k_{600} values, followed the same tidal pattern and were generally 2 orders of magnitude smaller for CH_4 (Table 1).

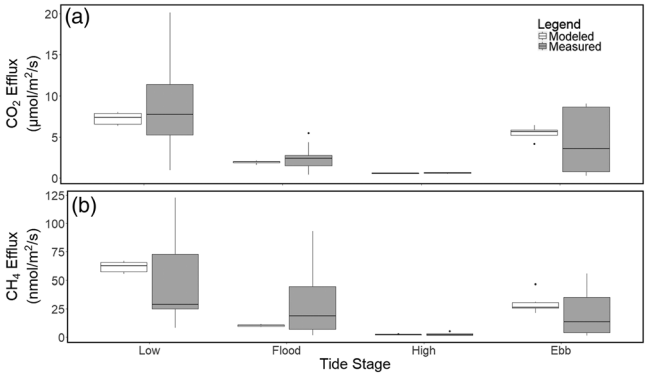

Figure 2. Boxplots comparing modeled and measured efflux of CO_2 (a) and CH_4 (b) divided by tide stage. All box plots by tide stage were significantly different from each other (Kruskal-Wallis test; $p < 0.05$) while there were no statistically significant differences between modeled and measured efflux within each tidal stage (Kruskal-Wallis test and bootstrap *t* test; $p > 0.05$).

Daily averages of pCO_2 in the creek (8,729 ± 622.2 μmol/mol) exhibited a seasonal trend with a peak in the *Maturity* phenophase (Figure 3a). Half-hourly averages of creek pCO_2 were highest at low tide (9,110 ± 810 μmol/mol), lowest at high tide (8,410 ± 776 μmol/mol), and roughly equal between flood (8,730 ± 805) and ebb tides (8,690 ± 780 μmol/mol) (Figures 4a–4d). Daily averages of modeled creek CO_2 efflux (3.7 ± 0.63 μmol/m^2/s), however, did not show a clear seasonal trend (Figure 3b). Half-hourly averages of modeled creek CO_2 efflux consistently showed higher variability at low tide (7.32 ± 0.52 μmol/m^2/s) than at high tide (0.56 ± 0.04 μmol/m^2/s) (Figures 4e–4h).

Table 1
Gas Transfer Velocities (k_{600}) of CO_2 and CH_4 by Tide Stage

GHG	High tide k_{600} (m/d)	Low tide k_{600} (m/d)	Ebb tide k_{600} (m/d)	Flood tide k_{600} (m/d)
CO_2	113.2 ± 17.8	1330.7 ± 626.5	1223.9 ± 328.65	363.2 ± 98.1
CH_4	2.48 ± 0.59	61.59 ± 14.2	29.2 ± 9.95	10.32 ± 4.52

Note. GHG means greenhouse gas.

Daily averages of pCH_4 in the creek (2,100 ± 782.9 μmol/mol) exhibited a seasonal trend with a peak in the *Maturity* phenophase and then declined at a slower rate than it peaked (Figure 3c). Half-hourly averages of pCH_4 also demonstrated a slight trend of being highest at high tide (2,180 ± 840 μmol/mol), lowest at low tide (1,900 ± 7.4 μmol/mol), and roughly equal between flood (2,130 ± 898 μmol/mol) and ebb tides (2,020 ± 708 μmol/mol) with slight differences in trends between phenophases (Figures 5a–5d). Daily averages of modeled CH_4 efflux (17.4 ± 6.9 nmol/m^2/s) held a similar seasonal pattern to pCH_4 albeit with a lower peak (Figure 3d). Half-hourly averages of modeled creek CH_4 emissions were consistently more variable at low tide (48.5 ± 17.1 nmol/m^2/s) than high tide (2.13 ± 0.78 nmol/m^2/s) (Figures 5e–5h). Data gaps in GHG concentrations were due to occasions when strong tides displaced the sensors from their original location (7.5% of the data).

We found a significant linear relationship ($p < 0.05$; $r^2 = 0.46$) between CO_2 efflux and. CH_4 efflux (Figure S2); consequently, supporting the performance of CCA to look how different environmental drivers influence these fluxes. We found statistically significant relationships (CCA; $p < 0.05$) between the daily averages of independent variables and modeled GHG efflux during the whole growing season and within each phenophase save for *Senescence* (due to data gaps). During the whole growing season, the CCA showed that dissolved oxygen and wind speed held relevant, hereby defined as a statistically significant correlation coefficient >|0.4|, negative correlations with creek CH_4 efflux (Figure 6a). Across phenophases, dissolved oxygen remained a relevant factor for creek CH_4 efflux except during the *Maturity* phenophase (Figures 6b–6d), and wind speed remained a relevant factor for CH_4 efflux only during the *Dormant* phenophase (Figure 6b). Salinity emerged as a relevant factor for CH_4 efflux during the *Dormant* and *Greenup* phenophases, solar radiation only during the *Dormant* phenophase, and temperature only during the *Greenup* phenophase (Figures 6b and 6c). During the *Dormant* phenophase, dissolved oxygen, wind speed, solar radiation, and salinity were also relevant factors for CO_2 efflux (Figure 6b). During the Maturity phenophase, turbidity was the only variable notably associated with either GHG (Figure 6d). No relevant correlations between any independent variables and creek CO_2 efflux for the whole growing season were found as CO_2 efflux's linear correlation coefficient with the dependent variate was only 0.22 (Figure 6a).

We further look at independent linear relationships and found no significant relationship between CO_2 efflux and temperature (Figure S3), but significant relationships between CH_4 efflux and dissolved oxygen

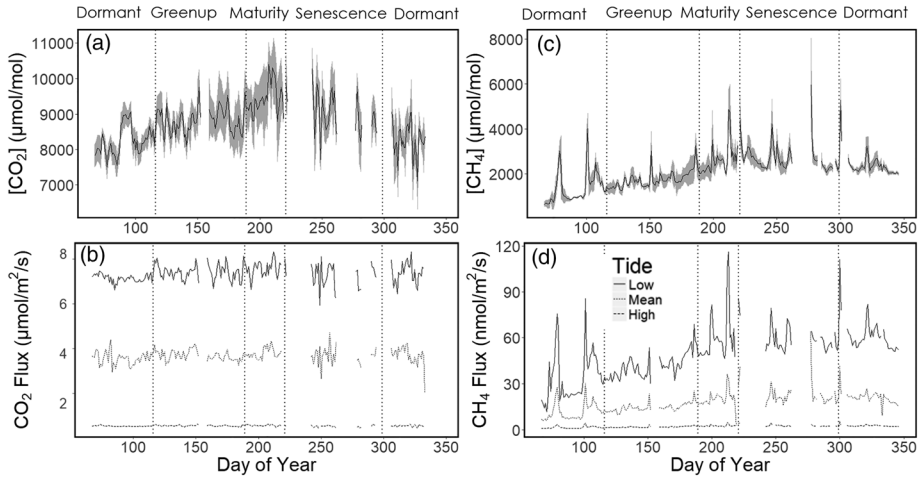

Figure 3. Time series of daily averages of creek pCO_2 (a) and pCH_4 (c). Time series of modeled CO_2 efflux (b) and modeled CH_4 efflux (d) divided into daily averages for high-tide and low-tide values, and a daily mean calculated with all available data. The shaded gray area (in a and c) represents the 95% confidence intervals for the daily average. The time series are divided by into *Dormant*, *Greenup*, *Maturity*, and *Senescence* phenophases marked by vertical dotted lines.

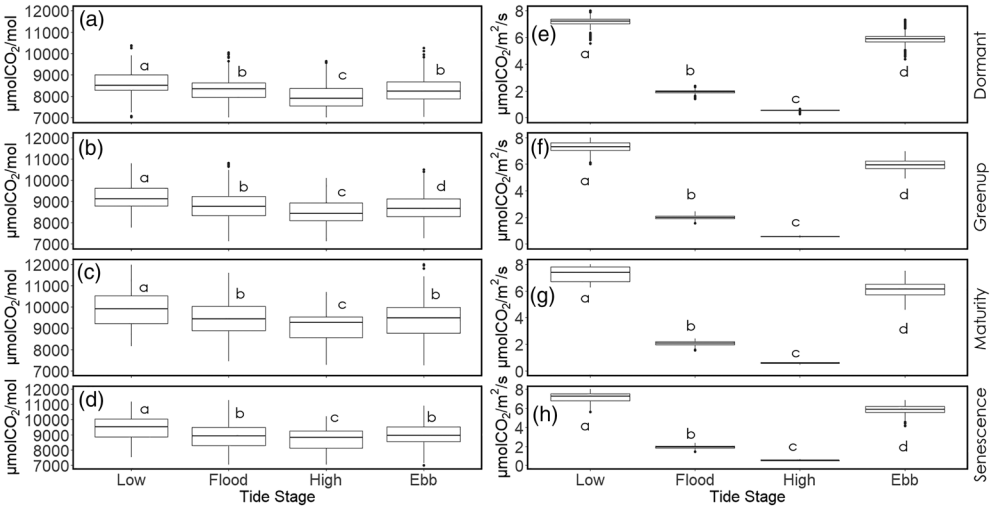

Figure 4. Box plots comparing CO_2 concentration (a–d) or CO_2 flux (e–h) between tide stages for each phenophase: *Dormant* (a, e), *Greenup* (b, f), *Maturity* (c, g), and *Senescence* (d, h). Different letters located above or below each box plot represent statistical significance ($p < 0.05$) among values in that panel.

($r^2 = -0.34$; Figure S4) and CH_4 efflux and wind speed ($r^2 = -0.23$; Figure S5), supporting the need to look at the multivariate interaction (i.e., using CCA) of these environmental factors on the GHG fluxes.

Statistically significant differences were found between ecosystem-scale, creek, and sediment efflux within each phenophase for CO_2 and between ecosystem and creek efflux within each phenophase for CH_4 (Figure 7, ANOVA; $p < 0.05$). Only CO_2 efflux measurements (for sediment and creek) taken at nighttime were considered for comparison with nighttime ecosystem-scale CO_2 efflux measurements (NEE). During the whole year, nighttime creek CO_2 efflux (3.6 ± 0.63 μmol/m^2/s) was significantly higher than nighttime sediment efflux (1.5 ± 1.23 μmol/m^2/s) but lower than nighttime NEE (5.4 ± 3.9 μmol/m^2/s). However, during the *Dormant* period, nighttime creek CO_2 efflux (3.7 ± 0.45 μmol/m^2/s) was higher than both nighttime sediment efflux (0.95 ± 0.81 μmol/m^2/s) and NEE (2.1 ± 1.1 μmol/m^2/s). Creek CH_4 efflux (17.5 ± 6.9 nmol/m^2/s) was consistently lower than ecosystem-scale CH_4 efflux (68.1 ± 52.3 nmol/m^2/s) across the whole growing season, with the gap between the two widening as the season progressed.

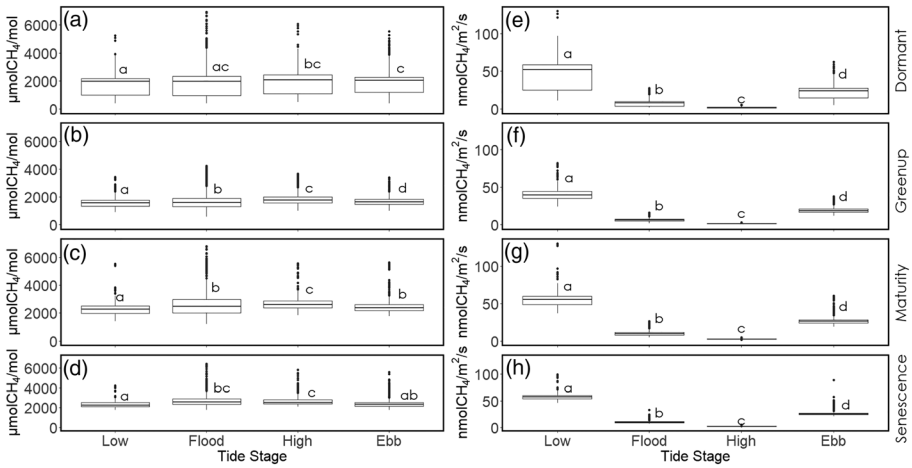

Figure 5. Box plots comparing pCH_4 (a–d) or CH_4 efflux (e–h) between tide stages for each phenophase: *Dormant* (a, e), *Greenup* (b, f), *Maturity* (c, g), and *Senescence* (d, h). Different letters above each box plot represent statistical significance ($p < 0.05$) among values in that panel.

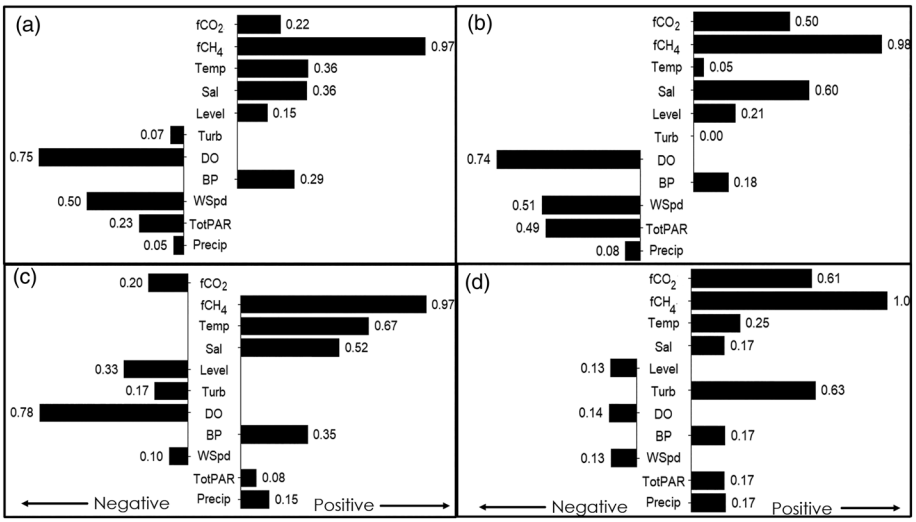

Figure 6. Results of a canonical correlation analysis (CCA) between measured environmental variables and modeled creek CO_2 and CH_4 efflux during the following: the whole growing season (a), *Dormant* phenophase (b), *Greenup* phenophase (c), the *Maturity* phenophase (d). The *Senescence* phenophase was found to not have any statistically significant relationships between factors ($p > 0.05$). Numbers represent the linear correlation coefficients between factors with negative correlation coefficients going to the left and positive correlation coefficients going to the right. fCO_2 is CO_2 efflux ($\mu mol/m^2/s$), fCH_4 is CH_4 efflux ($nmol/m^2/s$), temp is water temperature (°C), Sal is salinity (ppt), Level is water level (m), Turb is turbidity (NTU), DO is dissolved oxygen (mg/l), BP is barometric pressure (mb), WSpd is wind speed (m/s), TotPAR is total photosynthetically active radiation ($mmol/m^2$), and Precip is precipitation (mm).

4. Discussion

The first hypothesis, that GHG efflux from the creek would peak in the *Maturity* phenophase, was supported for CH_4 but not for CO_2 as the creek lacked significant seasonal variability for CO_2 efflux but showed some seasonal variability for CH_4 efflux (Figure 3). This differs from observations in temperate terrestrial environments such as forests where both CO_2 and CH_4 emissions exhibited strong seasonal trends driven by changing temperatures (Yvon-Durocher et al., 2014, 2012). Inland temperate aquatic environments like rivers have also exhibited seasonal trends in CO_2 efflux (Laruelle et al., 2015). However, the concentrations of both

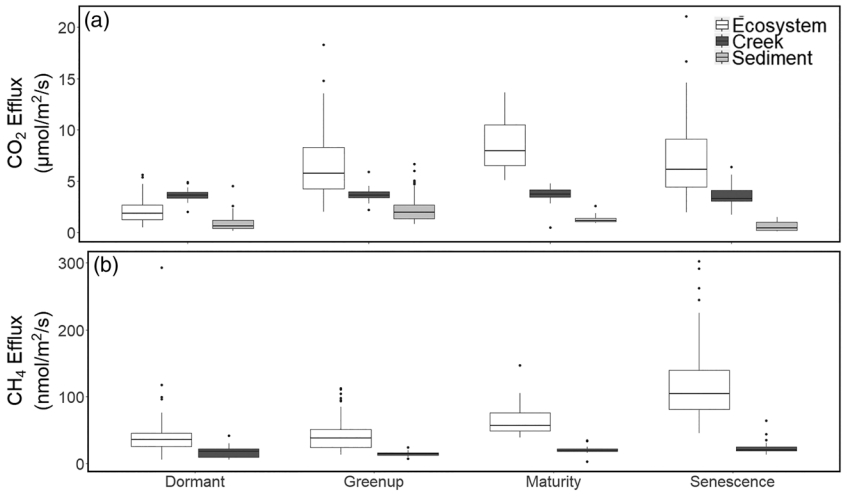

Figure 7. Box plots comparing ecosystem-scale CO_2 efflux (nighttime NEE), creek nighttime CO_2 efflux, and nighttime sediment CO_2 efflux (a). Box plots comparing ecosystem-scale and creek CH_4 fluxes (b). Box plots are arranged based on each phenophase. All box plots within each phenophase were significantly different from each other ($p < 0.05$). Sediment CH_4 efflux was not measured.

GHGs in the creek did exhibit more of a seasonal pattern than the efflux (Figure 3). The lack of a seasonal trend for GHG efflux compared to the concentrations suggests the influence of confounding and competing factors beyond the concentration gradient between water and air. These factors were tidally linked, likely influencing the gas transfer velocity (k; see below), as the efflux of both GHGs differed markedly by tidal stage (Figures 4 and 5). Both GHG effluxes also lacked the expected high correlations with water temperature (Figure 6), suggesting that creek GHG efflux has drivers that are fundamentally different from those of inland terrestrial and aquatic ecosystems. This lack of temperature dependency should be tested across other salt marsh creeks but, if it proves to be persistent, then this could be an important mathematical and conceptual formulation for ecosystem process models across terrestrial-aquatic interfaces.

The influence of tides may explain why the second hypothesis (that ebb and flood tides would have the highest GHG efflux) was only partially supported. One relevant tidal factor is likely water velocity changing with tide stage. Water velocity has been observed to increase the gas transfer velocity (k) of air-water gas efflux in terrestrial streams (Raymond et al., 2012) and estuaries (Jeffrey et al., 2018; Rosentreter et al., 2017). A higher k during flood and ebb tides may explain why there is a higher GHG efflux during those tide stages. Many tidal channels also experience tidal asymmetry between ebb and flood tides (Pethick, 1980) where one stage has a faster velocity than the other. This tidal asymmetry in velocity may explain the observed difference in flux magnitude between ebb and flood tides (Figures 2–5). However, low tide exhibited higher mean efflux than both ebb and flood tide despite its slower velocity. The difference in GHG efflux between low tide and other tides was substantially higher than the proportional difference in GHG concentrations (Figures 4 and 5). We highlight that flux models based on Fick's law of diffusion are very sensitive to diffusion coefficients (i.e., gas transfer velocity) rather than changes in concentrations (i.e., dc/dt or dc/dz) (Vargas & Allen, 2008). Consequently, this physical process (i.e., changes in gas transfer velocity) may be more predominant in controlling the surface efflux than changes in concentration within the water due to porewater/groundwater seepage or changes in benthic respiration or methanogenesis. Furthermore, it is likely that turbulence may be an additional tidal factor that affects GHG efflux in tidal creeks. As water level falls in a tidal channel, more flow is directed along the channel axis, rather than across, which generates higher turbulence between the creek bed and the water body (Ralston & Stacey, 2006). Laboratory experiments have demonstrated that increased turbulence at the bottom of water bodies 48–48.6 cm in depth increases the k at the surface (Herlina & Jirka, 2008). At low tide, the creek surface can range from 10–28 cm above the creek bed and thus the surface k may be more sensitive to turbulence changes at the creek bed. This suggests velocity-based GHG efflux models, as typical for inland streams, will not be accurate for tidal creeks without taking turbulence into account.

Standardized k_{600} values for CO_2 for all tide stages were 1 to 2 orders of magnitude higher than those observed in estuaries and deep (>1 m depth) rivers (Bianchi, 2006; Borges et al., 2004). High tide k_{600} values were similar to k_{600} values in shallow streams and rivers, flood tide values were 3 times higher, while low and ebb tide values were an order of magnitude higher than the highest k_{600} values in these shallow systems (Lorke et al., 2015; Raymond et al., 2012). CH_4 k_{600} values fell within the typical range for shallow streams and rivers save for low tide which averaged twice as high as the highest shallow system observations (Lorke et al., 2015). It is likely that tidal creeks have uniquely high k_{600} values due to their shallow depths, larger pCO_2 and pCH_4 values, and the dynamic shifting of velocity and turbulence (Herlina & Jirka, 2008; Ralston & Stacey, 2006; Raymond et al., 2012) due to tides.

The CCA allowed us to explore the third hypothesis, that CO_2 and CH_4 efflux would be interrelated and that dissolved oxygen and salinity would inhibit CH_4 efflux, at the annual scale and by phenophase. First, we found a relationship between CO_2 and CH_4 efflux (Figure S2) similar to what has been reported for ecosystem scale fluxes (Knox et al., 2019), termite mounds (Jamali et al., 2013), and from tree stems (Vargas & Barba, 2019). This relationship could represent the potential influence of CH_4 production and subsequent oxidation into CO_2 (Van der Nat et al., 1997), or the underlying environmental factors that jointly influence these GHG fluxes as explored with the CCA. We highlight that studies should consider exploring the potential confounding effects of multiple independent variables and the potential autocorrelation of dependent variables such as CO_2 and CH_4 efflux.

Our results from the CCA shows the multivariate relationship of environmental controls accounting for the interdependency of CO_2 and CH_4 fluxes. For example, dissolved oxygen had a negative relationship with

CH_4 efflux at the annual scale, but also during the *Dormant* and *Greenup* phenophases (Figure 6), likely due to the inhibiting effect of oxygen on methanogenesis (Poffenbarger et al., 2011; Tobias & Neubauer, 2009). At the annual scale, wind speed was also an important factor as higher wind speeds can produce more turbulence, aerate the water surface, and thus bring more dissolved oxygen into streams (Chu et al., 2003; Gualtieri et al., 2002). Salinity showed a positive relationship with CH_4 efflux during the *Dormant* and *Greenup* phenophases and no relevant relationships at the annual scale or for any other phenophase. This contrasts with the expected negative relationship that has been observed in salinity gradient studies and between salt marshes with differing salinity ranges (Bartlett et al., 2016; Poffenbarger et al., 2011). This apparent contradiction could be explained by tidal transport of CH_4 with the incoming flood tide (Figure 5) or the temporal variability of salinity within the creek being smaller in magnitude compared to the spatial variability within and between salt marshes. An additional explanation could be that CH_4 in marsh sediments is produced through the methylotrophic pathway in which sulfate reducing bacteria do not compete for substrate, as show in recent work (Seyfferth et al., 2020). Despite previous studies having found a strong relationship between temperature and soil CH_4 efflux (Westermann, 1993; Yvon-Durocher et al., 2014), our results only supported these observations during the *Greenup* phenophase. This may be due to tides having a strong influence on k, which in turn is a stronger control on creek CH_4 efflux than temperature influence.

We did not find a significant relationship between CO_2 efflux and temperature from the CCA (Figure 6) or using a simple linear regression approach (Figure S3). We attribute that the same physical controls that regulate CH_4 override any temperature response for CO_2 efflux. However, during the *Dormant* phenophase, dissolved oxygen, wind speed, solar radiation, and salinity had relevant relationships with CO_2 efflux. Both GHG effluxes also had high correlations with each other and the aforementioned parameters during the *Dormant* phenophase (Figure 6). Thus, the parameters with relevant correlations with CO_2 efflux may have emerged due to this positive relationship with CH_4 efflux, as hypothesized. Both GHG effluxes also held positive relationships with each other and turbidity during the *Maturity* phenophase. The turbidity relationship may represent a pulse of sediments and GHGs entering the creek from the banks with the two events of water level rise seen during the *Maturity* phenophase (Figure 1).

These results bring attention to the potential challenges of modeling GHG fluxes from tidal creeks since there appear to be confounding and competing factors for CH_4 efflux and no clear dominant factors for CO_2 efflux. Identifying consistent key drivers for soil CO_2 and CH_4 efflux under non-stationary conditions (e.g., during wetting-drying and freezing–thawing cycles) has also be proven to be challenging (Kim et al., 2012). Thus, there is a need to provide more information regarding GHGs pulses and trends across terrestrial and aquatic environments.

Nighttime creek CO_2 efflux was higher than nighttime sediment CO_2 efflux and represented a significant portion of ecosystem-scale CO_2 efflux (i.e., nighttime NEE). These results support the fourth hypothesis that the creek was a hot spot for CO_2 efflux. Our results support previous observations on point measurements of GHG efflux across different flowing waters of coastal wetlands but expand upon these observations by comparing automated measurements across water, sediments, and the ecosystem scale. For example, a river flowing through a salt marsh was found to have higher CO_2 emissions but slightly lower CH_4 emissions than the bare soil or marsh plants (Yang et al., 2017), which matches our comparatively low creek CH_4 efflux. However, it should be noted that our model does not incorporate ebullition of CH_4, as ebullition is a rapid episodic process (Joyce & Jewell, 2003) that was not captured during our manual measurements. Based on CH_4 ebullition studies of wetland sediments and streams, our results may be underestimating creek CH_4 efflux (Chanton et al., 1989; Crawford et al., 2014). It is also worth noting that comparisons of GHG efflux between top-down eddy covariance and bottom-up direct flux measurements often yield discrepancies due to the potential for top-down techniques to miss hotspot areas due to their shifting footprint (Barba et al., 2018). The tidal creeks of mangroves have also shown high pCO_2 and pCH_4 (Call et al., 2015; Linto et al., 2014), but gas transfer velocities *(k)* need to be developed to quantify the effective water-to-atmosphere efflux from these surfaces. Furthermore, this study builds on the evidence that inland streams and rivers have large CO_2 emissions globally (1.8 pG CO_2/year) relative to their surrounding ecosystems (Lauerwald et al., 2015; Raymond et al., 2013) by suggesting that tidal creeks are also emission hotspots within their

respective ecosystems. Therefore, it is critical to constrain the magnitude of water-to-atmosphere fluxes to reduce the large uncertainties in the carbon cycle associated to tidal wetlands (Hayes et al., 2018).

We postulate that higher CO_2 efflux at the creek may be due to lateral transport of CO_2 from the creek bank (i.e., sediments that get exposed during low tide) into the creek water (as a physical process driven by the tidal patterns) that increases the water-atmosphere CO_2 gradient (Koné & Borges, 2008). Of note is that creek CO_2 efflux during the *Dormant* period was disproportionately high, having a higher mean than ecosystem-scale CO_2 efflux. It is likely that lateral transport of CO_2 from sediments to the creek waters (promoted by tidal patterns) is persistent throughout the year and maintains high CO_2 concentrations and emissions from the tidal creek. The overall ecosystem CO_2 efflux (i.e., nighttime NEE) decreased during the *Dormant* period likely due to low *S. alterniflora* root respiration (Teal & Kanwisher, 1966) from plant senescence and low microbial heterotrophic respiration from lower temperatures (Yvon-Durocher et al., 2012; Zhang et al., 2013). Therefore, we propose that the influence of physical processes driven by tidal patterns should be included in process-based models for tidal salt marshes and should be taken into consideration when partitioning eddy covariance NEE into gross primary production and ecosystem respiration.

Tides can also promote the lateral transport of CH_4 stored in sediments to the creek. It has been reported that sediments at our study site can have CH_4 concentrations >50,000 μmol/mol (Seyfferth et al., 2020), so they can also be a source of CH_4 to the tidal creek. It was not uncommon to measure CH_4 concentrations at 2,000 μmol/mol (and up to > 6,000 μmol/mol) within the creek, so this opens the following question: Where does this CH_4 go? We postulate that tides promote lateral transport of CH_4 stored in sediments of salt marshes to the coastal ocean. This has been suggested as a mechanism for CH_4 transport in the North Sea of Germany from surrounding tidal flats (Osudar et al., 2015). This hypothesis must be tested across tidal ecosystems around the world.

Finally, the insights gained into the tidal processes affecting creek GHG efflux and its relationship to ecosystem-scale and sediment GHG fluxes would not be possible without high temporal resolution using automated measurements. Manual measurements can often miss rapid changes in ecological variables like dissolved oxygen (Banas et al., 2005) so automated measurements have been touted to help resolve uncertainties in sediments of salt marshes (Capooci et al., 2019), ecological, and carbon cycle models (Hamilton et al., 2015; Vargas et al., 2011). However, manual GHG flux measurements are urgently needed to understand the spatial variability and magnitudes of GHG fluxes across different landscape features of tidal salt marshes around the world. Only a synergistic effort across the scientific community will provide the much-needed information to accurately account for the contribution of coastal wetlands to the global carbon cycle (Harden et al,. 2018; Ward et al., 2020).

5. Conclusions

This study offered unprecedented information of GHG dynamics in a tidal creek using high temporal resolution automated measurements. Both GHG effluxes from the creek did not exhibit the expected strong temperature-driven seasonal trend, with CO_2 efflux having no trend and CH_4 efflux having a moderate one. We postulate that the physical effects of tidal changes (velocity, turbulence) overshadows the influence of water temperature in determining magnitudes of GHG efflux. Dissolved oxygen exhibited a negative relationship with CH_4 efflux, as expected, while salinity did not due to confounding factors or a methanogenesis pathway that is not salinity dependent. CO_2 efflux had no consistent drivers across the year, suggesting it will be difficult to model and predict throughout the year. The creek exhibited 2 times higher CO_2 efflux than the sediments and made up around 66% of the overall CO_2 emissions from the marsh, suggesting creeks are CO_2 emission hotspots within the salt marsh landscape. We postulate that tidal patterns influence the lateral transport of marsh sediment CO_2 and CH_4 into the creek water, and because of the supersaturation of pCO_2 and pCH_4 in the water, there is likely a lateral transport to the coastal ocean. The dynamics of GHG fluxes in tidal marshes are regulated in a fundamentally different way than from terrestrial ecosystems; thus, future ecosystem process-based models should evaluate current assumptions to improve the representation of terrestrial-aquatic interfaces.

Data Availability Statements

Plant phenology data can be downloaded from https://phenocam.sr.unh.edu under the site name *stjones*. Eddy covariance CO_2 and CH_4 flux data can be downloaded from https://ameriflux.lbl.gov/ under the site ID US-StJ. Meteorological data can be downloaded from https://cdmo.baruch.sc.edu/ under the site name DELSJMET. Creek pCO_2 and pCH_4, modeled and measured creek CO_2 and CH_4 efflux, soil CO_2 efflux and concentration, and water quality data can be downloaded from Figshare (10.6084/m9.figshare.12340580.v1).

Acknowledgments

This study was primarily supported by NSF Grant 1652594 to R. V. We would also like to thank Kari Saint-Laurent and Mike Mensinger for support of our work at the study site; and Daniel Warner, Josep Barba, and Ricardo Llamas help in collecting manual GHG flux measurements. A. V. L. acknowledges support from the National Council for Science and Technology (CONACYT) fellowship (240634/440832) and the Delaware Environmental Graduate Fellowship (DENIN). M. C. acknowledges support from DENIN Environmental Fellowship, as well as an NSF Graduate Research Fellowship (1247394). C. M. acknowledges support from the Delaware Sea Grant College Program (DESG) with funds from the National Oceanic and Atmospheric Administration (NOAA) Office of Sea Grant, U.S. Department of Commerce, under NOAA Grant NA18OAR4170086 and DESG. A. L. S. acknowledges support from NSF Grant 1759879.

References

Banas, D., Grillas, P., Auby, I., Lescuyer, F., Coulet, E., Moreteau, J. C., & Millet, B. (2005). Short time scale changes in underwater irradiance in a wind-exposed lagoon (Vaccarès lagoon, France): Efficiency of infrequent field measurements of water turbidity or weather data to predict irradiance in the water column. *Hydrobiologia*, *551*(1), 3–16. https://doi.org/10.1007/s10750-005-4446-1

Barba, J., Cueva, A., Bahn, M., Barron-Gaffordd, G. A., Bond-Lamberty, B., Hanson, P. J., Jaimes, A., et al. (2018). Comparing ecosystem and soil respiration: Review and key challenges of tower-based and soil measurements. *Agricultural and Forest Meteorology*, *249*(February), 434–443.

Bartlett, K. B., Bartlett, D. S., Harriss, R. C., Sebacher, D. I., Biogeochemistry, S., & Sebacher, D. I. (2016). Methane emissions along a salt marsh salinity gradient. *Biogeochemistry*, *4*(3), 183–202. https://doi.org/10.1007/BF02187365

Baumann, H., Wallace, R. B., Tagliaferri, T., & Gobler, C. J. (2015). Large natural pH, CO^2 and O^2 fluctuations in a temperate tidal salt marsh on diel, seasonal, and interannual time scales. *Estuaries and Coasts*, *38*(1), 220–231. https://doi.org/10.1007/s12237-014-9800-y

Bianchi, T. S. (2006). *Dissolved gases in water in biogeochemistry of estuaries* (pp. 84–100). Oxford, UK: Oxford University Press.

Bond-lamberty, B., Bailey, V. L., Chen, M., Gough, C. M., & Vargas, R. (2018). Globally rising soil heterotrophic respiration over recent decades. *Nature*, *560*, 80–83. https://doi.org/10.1038/s41586-018-0358-x

Borges, A. V., Vanderborght, J. P., Schiettecatte, L. S., Gazeau, F., Ferron-Smith, S., Delille, B., & Frankignoulle, M. (2004). Variability of the gas transfer velocity of CO_2 in a macrotidal estuary (the Scheldt). *Estuaries*, *27*(4), 593–603. https://doi.org/10.1007/BF02907647

Call, M., Maher, D. T., Santos, I. R., Ruiz-Halpern, S., Mangion, P., Sanders, C. J., et al. (2015). Spatial and temporal variability of carbon dioxide and methane fluxes over semi-diurnal and spring-neap-spring timescales in a mangrove creek. *Geochimica et Cosmochimica Acta*, *150*, 211–225. https://doi.org/10.1016/j.gca.2014.11.023

Capooci, M., Barba, J., Seyfferth, A. L., & Vargas, R. (2019). Experimental influence of storm-surge salinity on soil greenhouse gas emissions from a tidal salt marsh. *Science of the Total Environment*, *686*, 1164–1172. https://doi.org/10.1016/j.scitotenv.2019.06.032

Chanton, J. P., Martens, C. S., & Kelley, C. A. (1989). Gas transport from methane-saturated, tidal freshwater and wetland sediments. *Limnology and Oceanography*, *34*(5), 807–819.

Chmura, G. L., Anisfeld, S. C., Cahoon, D. R., & Lynch, J. C. (2003). Global carbon sequestration in tidal, saline wetland soils. *Global Biogeochemical Cycles*, *17*(4), 1111. https://doi.org/10.1029/2002GB001917

Chmura, G. L., Kellman, L., & Guntenspergen, G. R. (2011). The greenhouse gas flux and potential global warming feedbacks of a northern macrotidal and microtidal salt marsh. *Environmental Research Letters*, *6*(4), 044016. https://doi.org/10.1088/1748-9326/6/4/044016

Chu, C. R., Jirka, G. H., & Asce, F. (2003). Wind and stream flow induced reaeration. *Journal of Environmental Engineering*, *129*, 1129–1136.

Cox, T. & Schepers, L. (2017). Tides: Quasi-periodic time series characteristics. R package version 2.0. https://CRAN.R-project.org/package=Tides

Crawford, J. T., Stanley, E. H., Spawn, A. S., Finlay, J. C., Loken, L. C., & Striegel, R. G. (2014). Ebullitive methane emissions from oxygenated wetland streams. *Global Change Biology*, *20*(11), 3408–3422. https://doi.org/10.1111/gcb.12614

Dausse, A., Garbutt, A., Norman, L., Papadimitriou, S., Jones, L. M., Robins, P. E., & Thomas, D. N. (2012). Biogeochemical functioning of grazed estuarine tidal marshes along a salinity gradient. *Estuarine, Coastal and Shelf Science*, *100*, 83–92. https://doi.org/10.1016/j.ecss.2011.12.037

Delaware Department of Natural Resources and Environmental Control (1999). *Delaware national estuarine research reserve estuarine profile*. Dover, DE: National Oceanic and Atmospheric Administration.

Desai, A. R. (2010). Climatic and phenological controls on coherent regional interannual variability of carbon dioxide flux in a heterogeneous landscape. *Journal of Geophysical Research*, *115*, G00J02. https://doi.org/10.1029/2010JG001423

Fagherazzi, S., Wiberg, P. L., Temmerman, S., Struyf, E., Zhao, Y., & Raymond, P. A. (2013). Fluxes of water, sediments, and biogeochemical compounds in salt marshes. *Ecological Processes*, *2*(1), 3. https://doi.org/10.1186/2192-1709-2-3

Filippa, G., Cremonese, E., Migliavacca, M., Galvagno, M., Forkel, M., Wingate, L., et al. (2016). Phenopix: A R package for image-based vegetation phenology. *Agricultural and Forest Meteorology*, *220*, 141–150. https://doi.org/10.1016/j.agrformet.2016.01.006

Flanagan, L. B. (2009). Phenology of plant production in the Northwestern Great Plains: Relationships with carbon isotope discrimination, net ecosystem productivity and ecosystem respiration. In A. Noormets (Ed.), *Phenology of Ecosystem Processes* (169–185). New York, NY: Springer.

Forbrich, I., & Giblin, A. E. (2015). Marsh-atmosphere CO_2 exchange in a New England salt marsh. *Journal of Geophysical Research: Biogeosciences*, *120*, 1825–1838. https://doi.org/10.1002/2015JG003044

Forbrich, I., Giblin, A. E., & Hopkinson, C. S. (2018). Constraining marsh carbon budgets using long-term C burial and contemporary atmospheric CO_2 fluxes. *Journal of Geophysical Research: Biogeosciences*, *123*, 867–878. https://doi.org/10.1002/2017JG004336

Gillespie, A. R., Kahle, A. B., & Walker, R. E. (1987). Color enhancement of highly correlated images. II. Channel ratio and "chromaticity" transformation techniques. *Remote Sensing of Environment*, *22*(3), 343–365. https://doi.org/10.1016/0034-4257(87)90088-5

González, I. & Déjean, S. (2012). CCA: Canonical correlation analysis. R package version 1.2.https://CRAN.R-project.org/package=CCA

Greenwood, D. J. (1961). The effect of oxygen concentration on the decomposition of organic materials in soil. *Plant and Soil*, *14*(4), 360–376.

Gualtieri, C., Gualtieri, P., & Doria, G. P. (2002). Dimensional analysis of reaeration rate in streams. *Journal of Environmental Engineering*, *128*(1), 12–18.

Hamilton, D. P., Carey, C. C., Arvola, L., Arzberger, P., Cole, J. J., Gaiser, E., et al. (2015). A Global Lake Ecological Observatory Network (GLEON) for synthesising high-frequency sensor data for validation of deterministic ecological models. *Inland Waters*, *5*(1), 49–56. https://doi.org/10.5268/IW-5.1.566

Harden, J. W., Hugelius, G., Ahlström, A., Blankinship, J. C., Bond-Lamberty, B., Lawrence, C. R., et al. (2018). Networking our science to characterize the state, vulnerabilities, and management opportunities of soil organic matter. *Global Change Biology*, *24*(2), e705–e718. https://doi.org/10.1111/gcb.13896

Hayes, D. J., Vargas, R., Alin, S. R., Conant, R. T., Hutyra, L. R., Jacobson, A. R., et al. (2018). Chapter 2: The North American carbon budget. In N. Cavallaro, G. Shrestha, R. Birdsey, M. A. Mayes, R. G. Najjar, S. C. Reed, et al. (Eds.), *Second State of the Carbon Cycle Report (SOCCR2): A sustained assessment report* (pp. 71–108). Washington, DC, USA: U.S. Global Change Research Program; 2018. https://doi.org/10.7930/SOCCR2.2018.Ch2

Herlina, A., & Jirka, G. H. (2008). Experiments on gas transfer at the air-water interface induced by oscillating grid turbulence. *Journal of Fluid Mechanics*, *594*, 183–208. https://doi.org/10.1017/S0022112007008968

Howard, J., Sutton-Grier, A., Herr, D., Kleypas, J., Landis, E., Mcleod, E., et al. (2017). Clarifying the role of coastal and marine systems in climate mitigation. *Frontiers in Ecology and the Environment*, *15*(1), 42–50. https://doi.org/10.1002/fee.1451

Huertas, I. E., Flecha, S., Figuerola, J., Costas, E., & Morris, E. P. (2017). Effect of hydroperiod on CO^2 fluxes at the air-water interface in the Mediterranean coastal wetlands of Doñana. *Journal of Geophysical Research: Biogeosciences*, *122*, 1615–1631. https://doi.org/10.1002/2017JG003793

Jamali, H., Livesley, S., Hutley, L. B., Fest, B., & Arndt, S. (2013). The relationships between termite mound CH_4/CO_2 emissions and internal concentration ratios are species specific. *Biogeosciences*, *10*(4), 2229–2240.

Jeffrey, L. C., et al. (2018). The spatial and temporal drivers of pCO_2, pCH_4 and gas transfer velocity within a subtropical estuary. Estuarine, *Coastal and Shelf Science*.

Jones, S. F., Stagg, C. L., Krauss, K. W., & Hester, M. W. (2018). Flooding alters plant-mediated carbon cycling independently of elevated atmospheric CO_2 concentrations. *Journal of Geophysical Research: Biogeosciences*, *123*, 1976–1987. https://doi.org/10.1029/2017JG004369

Joyce, J., & Jewell, P. W. (2003). Physical controls on methane ebullition from reservoirs and lakes. *Environmental and Engineering Geoscience*, *9*(2), 167–168.

Kang, X., Hao, Y., Cui, X., Chen, H., Huang, S., Du, Y., et al. (2016). Variability and changes in climate, phenology, and gross primary production of an alpine wetland ecosystem. *Remote Sensing*, *8*(5), 391.

Kim, D. G., Vargas, R., Bond-Lamberty, B., & Turetsky, M. R. (2012). Effects of soil rewetting and thawing on soil gas fluxes: A review of current literature and suggestions for future research. *Biogeosciences*, *9*(7), 2459–2483.

Kirwan, M. L., Guntenspergen, G. R., & Langley, J. A. (2014). Temperature sensitivity of organic-matter decay in tidal marshes. *Biogeosciences*, *11*(17), 4801–4808. https://doi.org/10.5194/bg-11-4801-2014

Knox, S. H., Jackson, R. B., Poulter, B., McNicol, G., Fluet-Chouinard, E., Zhang, Z., et al. (2019). FLUXNET-CH_4 synthesis activity: Objectives, observations, and future directions. *Bulletin of the American Meteorological Society*.

Koné, Y. J. M., & Borges, A. V. (2008). Dissolved inorganic carbon dynamics in the waters surrounding forested mangroves of the Ca Mau Province (Vietnam). *Estuarine, Coastal and Shelf Science*, *77*(3), 409–421. https://doi.org/10.1016/j.ecss.2007.10.001

Laruelle, G. G., Lauerwald, R., Rotschi, J., Raymond, P. A., Hartmann, J., & Regnier, P. (2015). Seasonal response of air–water CO_2 exchange along the land–ocean aquatic continuum of the northeast North American coast. *Biogeosciences*, *12*, 1447–1458. https://doi.org/10.5194/bg-12-1447-2015

Lauerwald, R., Laruelle, G. G., Hartmann, J., Ciais, P., & Regnier, P. A. G. (2015). Spatial patterns in CO_2 evasion from the global river network. *Global Biogeochemical Cycles*, *29*, 534–554. https://doi.org/10.1002/2014GB004941

Linto, N., Barnes, J., Ramachandran, R., Divia, J., Ramachandran, P., & Upstill-Goddard, R. C. (2014). Carbon dioxide and methane emissions from mangrove-associated waters of the Andaman Islands, Bay of Bengal. *Estuaries and Coasts*, *37*(2), 381–398. https://doi.org/10.1007/s12237-013-9674-4

Lorke, A., Bodmer, P., Noss, C., Alshboul, Z., Koschorrek, M., Somlai-Haase, C., et al. (2015). Drifting versus anchored flux chambers for measuring greenhouse gas emissions from running waters. *Biogeosciences*, *12*(23), 7013–7024. https://doi.org/10.5194/bg-12-7013-2015

Macreadie, P. I., Hughes, A. R., & Kimbro, D. L. (2013). Loss of "blue carbon" from coastal salt marshes following habitat disturbance. *PLoS ONE*, *8*(7), 1, e69244–8. https://doi.org/10.1371/journal.pone.0069244

Mahecha, M. D., Reichstein, M., Carvalhais, N., Lasslop, G., Lange, H., Seneviratne, S. I., et al. (2010). Global convergence in the temperature sensitivity of respiration at ecosystem level. *Science*, *329*(5993), 838–840. https://doi.org/10.1126/science.1189587

McLeod, E., Chmura, G. L., Bouillon, S., Salm, R., Björk, M., Duarte, C. M., et al. (2011). A blueprint for blue carbon: Toward an improved understanding of the role of vegetated coastal habitats in sequestering CO_2. *Frontiers in Ecology and the Environment*, *9*(10), 552–560. https://doi.org/10.1890/110004

Moffett, K. B., Wolf, A., Berry, J. A., & Gorelick, S. M. (2010). Salt marsh-atmosphere exchange of energy, water vapor, and carbon dioxide: Effects of tidal flooding and biophysical controls. *Water Resources Research*, *46*, W10525. https://doi.org/10.1029/2009WR009041

Moseman-Valtierra, S. (2012). Reconsidering the climatic role of marshes: Are they sinks or sources of greenhouse gases? In *Marshes: Ecology, management and conservation* (pp. 1–48). Hauppauge, NY, USA: Nova Scientific Publishers.

Neubauer, S. C., & Anderson, I. C. (2003). Transport of dissolved inorganic carbon from a tidal freshwater marsh to the York River estuary. *Limnology and Oceanography*, *48*(1), 299–307.

Osudar, R., Matou, A., Alawi, M., Wagner, D., & Bussmann, I. (2015). Environmental factors affecting methane distribution and bacterial methane oxidation in the German Bight (North Sea). *Estuarine, Coastal and Shelf Science*, *160*, 10–21. https://doi.org/10.1016/j.ecss.2015.03.028

Pearson, A. J., Pizzuto, J. E., & Vargas, R. (2016). Influence of run of river dams on floodplain sediments and carbon dynamics. *Geoderma*, *272*, 51–63. https://doi.org/10.1016/j.geoderma.2016.02.029

Pendleton, L., Donato, D. C., Murray, B. C., Crooks, S., Jenkins, W. A., Sifleet, S., et al. (2012). Estimating global "blue carbon" emissions from conversion and degradation of vegetated coastal ecosystems. *PLoS ONE*, *7*(9), e43542. https://doi.org/10.1371/journal.pone.0043542

Pethick, J. S. (1980). Velocity surges and asymmetry in tidal channels. *Estuarine and Coastal Marine Science*, *11*(3), 331–345. https://doi.org/10.1016/S0302-3524(80)80087-9

Poffenbarger, H. J., Needelman, B. A., & Megonigal, J. P. (2011). Salinity influence on methane emissions from tidal marshes. *Wetlands*, *31*(5), 831–842. https://doi.org/10.1007/s13157-011-0197-0

Raich, J. W., & Schlesinger, W. H. (1992). The global carbon dioxide flux in soil respiration and its relationship to vegetation and climate. *Tellus*, *44*, 81–99.

Ralston, D. K., & Stacey, M. T. (2006). Shear and turbulence production across subtidal channels. *Journal of Marine Research*, *64*(1), 147–171.

Raymond, P. A., Hartmann, J., Lauerwald, R., Sobek, S., McDonald, C., Hoover, M., et al. (2013). Global carbon dioxide emissions from inland waters. *Nature*, *503*(7476), 355–359. https://doi.org/10.1038/nature12760

Raymond, P. A., Zappa, C. J., Butman, D., Bott, T. L., Potter, J., Mulholland, P., et al. (2012). Scaling the gas transfer velocity and hydraulic geometry in streams and small rivers. *Limnology and Oceanography: Fluids and Environments*, *2*(1), 41–53. https://doi.org/10.1215/21573689-1597669

Richardson, A. D., Andy, B. T., Ciais, P., Delbart, N., Friedl, M. A., Gobron, N., et al. (2010). Influence of spring and autumn phenological transitions on forest ecosystem productivity. *Philospohical Transactions of the Royal Society B*, *365*(1555), 3227–3246. http://doi.org/10.1098/rstb.2010.0102

Risk, D., Nickerson, N., Creelman, C., Mcarthur, G., & Owens, J. (2011). Agricultural and forest meteorology forced diffusion soil flux: A new technique for continuous monitoring of soil gas efflux. *Agricultural and Forest Meteorology*, *151*(12), 1622–1631. https://doi.org/10.1016/j.agrformet.2011.06.020

Rosentreter, J., Maher, D. T., Ho, D. T., Call, M., Barr, J. G., & Eyre, B. D. (2017). Spatial and temporal variability of CO_2 and CH_4 gas transfer velocities and quantification of the CH_4 microbubble flux in mangrove dominated estuaries. *Limnology and Oceanography*, *62*(2), 561–578. https://doi.org/10.1002/lno.10444

Ruiz-Fernández, A. C., Carnero-Bravo, V., Sanchez-Cabeza, J. A., Pérez-Bernal, L. H., Amaya-Monterrosa, O. A., Bojórquez-Sánchez, S., et al. (2018). Carbon burial and storage in tropical salt marshes under the influence of sea level rise. *Science of the Total Environment*, *630*, 1628–1640. https://doi.org/10.1016/j.scitotenv.2018.02.246

Sadat-Noori, M., et al. (2015). Groundwater discharge as a source of dissolved carbon and greenhouse gases in a subtropical estuary. *Estuaries and Coasts*, *39*(3), 639–656.

Santos, I. R., et al. (2012). The driving forces of porewater and groundwater flow in permeable coastal sediments: A review. *Estuarine, Coastal and Shelf Science*, *98*, 1–15.

Seyednasrollah, B., Young, A.M., Hufkens, K., Milliman, T., Friedl, M.A., Frolking, S., ... Zona, D. (2019). PhenoCam dataset v2.0: Vegetation phenology from digital camera imagery, 2000-2018. ORNL DAAC, Oak Ridge, Tennessee, USA. https://doi.org/10.3334/ORNLDAAC/1674

Seyfferth, A. L., Bothfeld, F., Vargas, R., Stuckey, J. W., Wang, J., Kearns, K., et al. (2020). Spatial and temporal heterogeneity of geochemical controls on carbon cycling in a tidal salt marsh. *Geochimica et Cosmochimica Acta*. https://doi.org/10.1016/j.gca.2020.05.013

Small, T. D., Ide, M. R., & Keesee, J. M. (2012). *CDMO NERR SWMP Data Management Manual (Version 6.4) NOAA National Estuarine Research Reserve, Central Data Management Office, Baruch Marine Laboratory, University of South Carolina*. Georgetown, South Carolina

Soil Survey Staff NRCS, United States Department of Agriculture. (2019) Web soil survey. https://websoilsurvey.sc.egov.usda.gov/App/HomePage.htm

Teal, J. M., & Kanwisher, J. W. (1966). Gas transport in the marsh grass, *Spartina alterniflora*. *Journal of Experimental Botany*, *17*(2), 355–361. https://doi.org/10.1093/jxb/17.2.355

Thomas, B. (1984). *Canonical correlation analysis: Uses and interpretation*. Thousand Oaks, California: Sage Publications.

Tobias, C., & Neubauer, S. (2009). *Chapter 16—Salt marsh biogeochemistry—An overview. Coastal Wetlands: An integrated ecosystem approach (first edit, vol. 76)*. New York: Elsevier. https://doi.org/10.1016/B978-0-444-53103-2.00016-8

Tong, C., Huang, J. F., Hu, Z. Q., & Jin, Y. F. (2013). Diurnal variations of carbon dioxide, methane, and nitrous oxide vertical fluxes in a subtropical estuarine marsh on neap and spring tide days. *Estuaries and Coasts*, *36*, 633–642. https://doi.org/10.1007/s12237-013-9596-1

Tong, C., Wang, W.-Q., Zeng, C.-S., & Marrs, R. (2010). Methane (CH_4) emission from a tidal marsh in the Min River estuary, Southeast China. *Journal of Environmental Science and Health Part A, Toxic/Hazardous Substances & Environmental Engineering*, *45*(4), 506–516. https://doi.org/10.1080/10934520903542261

Van Dam, B. R., Edson, J. B., & Tobias, C. (2019). Parameterizing air-water gas exchange in the shallow, microtidal New River estuary. *Journal of Geophysical Research: Biogeosciences*, *124*, 2351–2363. https://doi.org/10.1029/2018JG004908

Van der Nat, F. J. W. A., De Brouwer, J., Middelburg, J. J., & Laanbroek, H. J. (1997). Spatial distribution and inhibition by ammonium of methane oxidation in intertidal freshwater marshes. *Applied and Environmental Microbiology*, *63*(12), 4734–4740.

Vargas, R., & Allen, M. F. (2008). Diel patterns of soil respiration in a tropical forest after Hurricane Wilma. *Journal of Geophysical Research*, *113*, G03021. https://doi.org/10.1029/2007JG000620

Vargas, R., & Barba, J. (2019). Greenhouse gas fluxes from tree stems. *Trends in Plant Science*, *24*(4), 296–299. https://doi.org/10.1016/j.tplants.2019.02.005

Vargas, R., Carbone, M. S., Reichstein, M., & Baldocchi, D. D. (2011). Frontiers and challenges in soil respiration research: from measurements to model-data integration. *Biogeochemistry*, *102*, 1–13. https://doi.org/10.1007/s10533-010-9462-1

Vázquez-Lule, A., Colditz, R., Herrera-Silveira, J., Guevara, M., Rodríguez-Zúñiga, M. T., Cruz, I., et al. (2019). Greenness trends and carbon stocks of mangroves across Mexico. *Environmental Research Letters*, *14*(7), 075010.

Wang, Z. A., & Cai, W. J. (2004). Carbon dioxide degassing and inorganic carbon export from a marsh-dominated estuary (the Duplin River): A marsh CO_2 pump. *Limnology and Oceanography*, *49*(2), 341–354. https://doi.org/10.4319/lo.2004.49.2.0341

Wang, Z. A., Kroeger, K. D., Ganju, N. K., Gonneea, M. E., & Chu, S. N. (2016). Intertidal salt marshes as an important source of inorganic carbon to the coastal ocean. *Limnology and Oceanography*, *61*(5), 1916–1931. https://doi.org/10.1002/lno.10347

Wanninkhof, R. (2014). Relationship between wind speed and gas exchange over the ocean revisited. *Limnology and Oceanography: Methods*, *12*, 351–362.

Ward, N. D., Megonigal, J. P., Bond-Lamberty, B., Bailey, V. L., Butman, D., Canuel, E. A., et al. (2020). Representing the function and sensitivity of coastal interfaces in earth system models. *Nature Communications*, *11*(1), 2458. https://doi.org/10.1038/s41467-020-16236-2

Warner, D. L., Villarreal, S., Mcwilliams, K., Inamdar, S., & Vargas, R. (2017). Carbon dioxide and methane fluxes from tree stems, coarse woody debris, and soils in an upland temperate forest. *Ecosystems*, *20*(6), 1205–1216. https://doi.org/10.1007/s10021-016-0106-8

Westermann, P. (1993). Temperature regulation of methane in wetlands. *Chemosphere*, *26*, 321–328.

Wu, C., Chen, J. M., Black, T. A., Price, D. T., Kurz, W. A., Desai, A. R., et al. (2013). Interannual variability of net ecosystem productivity in forests is explained by carbon flux phenology in autumn. *Global Ecology and Biogeography*, *22*, 994–1006. https://doi.org/10.1111/geb.12044

Yang, W. B., Yuan, C. S., Tong, C., Yang, P., Yang, L., & Huang, B. Q. (2017). Diurnal variation of CO_2, CH_4, and N_2O emission fluxes continuously monitored in-situ in three environmental habitats in a subtropical estuarine wetland. *Marine Pollution Bulletin*, *119*(1), 289–298. https://doi.org/10.1016/j.marpolbul.2017.04.005

Yvon-Durocher, G., Allen, A. P., Bastviken, D., Conrad, R., Gudasz, C., St-Pierre, A., et al. (2014). Methane fluxes show consistent temperature dependence across microbial to ecosystem scales. *Nature*, *507*(7493), 488–491. https://doi.org/10.1038/nature13164

Yvon-Durocher, G., Caffrey, J. M., Cescatti, A., Dossena, M., Del Giorgio, P., Gasol, J. M., et al. (2012). Reconciling the temperature dependence of respiration across timescales and ecosystem types. *Nature*, *487*(7408), 472–476. https://doi.org/10.1038/nature11205

Zhang, Q., Lei, H. M., & Yang, D. W. (2013). Seasonal variations in soil respiration, heterotrophic respiration and autotrophic respiration of a wheat and maize rotation cropland in the North China plain. *Agricultural and Forest Meteorology*, *180*, 34–43. https://doi.org/10.1016/j.agrformet.2013.04.028

Zhong, Q., Du, Q., Gong, J., Zhang, C., & Wang, K. (2013). Effects of in situ experimental air warming on the soil respiration in a coastal salt marsh reclaimed for agriculture. *Plant and Soil*, *371*(1–2), 487–502. https://doi.org/10.1007/s11104-013-1707-z

Erratum

In the originally published version of this article, a typesetting error caused the title to erroneously publish without “a” between “From” and “Temperate.” The title has since been corrected, and this version may be considered the authoritative version of record.